Journal of Physics: Condensed Matter

PAPER

Crystal structure and physical properties of the two stannides $EuPdSn_2$ and $YbPdSn_2$

To cite this article: I urlík *et al* 2018 *J. Phys.: Condens. Matter* **30** 495802

IOP Publishing Journal of Physics: Condensed Matter
J. Phys.: Condens. Matter **30** (2018) 495802 (6pp) https://doi.org/10.1088/1361-648X/aae7ae

Crystal structure and physical properties of the two stannides $EuPdSn_2$ and $YbPdSn_2$

I Čurlík[1], M Giovannini[2], F Gastaldo[3], A M Strydom[4], M Reiffers[1,5] and J G Sereni[6]

[1] Faculty of Humanities and Natural Sciences, University of Prešov, 17. novembra 1, Prešov, Slovakia
[2] Department of Physics, University of Genova, Via Dodecaneso 33, Genova, Italy
[3] Department of Chemistry, University of Genova, Via Dodecaneso 31, Genova, Italy
[4] Highly Correlated Matter Research Group, Department of Physics, University of Johannesburg, PO Box 524, Auckland Park 2006, South Africa
[5] Institute of Experimental Physics, Slovak Academy of Science, Watsonova 47, Košice, Slovakia
[6] Department of Physics, CAB-CNEA, CONICET, 8400 San Carlos de Bariloche, Argentina

E-mail: ivan.curlik@unipo.sk

Received 30 July 2018, revised 2 October 2018
Accepted for publication 11 October 2018
Published 15 November 2018

Abstract

We report on synthesis, crystal structure and physical properties of the isotypic compounds $YbPdSn_2$ and $EuPdSn_2$ crystallizing in the $MgCuAl_2$-type structure. In both stannides a divalent state of respective rare earth element was found from analysis of the magnetic susceptibilities. Whereas in $YbPdSn_2$ only weak paramagnetic behaviour is observed, in $EuPdSn_2$ a long-range magnetic phase transition occurs at 12.5 K with complex magnetic behaviour evidenced by magnetic susceptibity and specific heat measurements. Under the influence of magnetic field, the magnetic behaviour was found to evolve from an antiferromagnetic to a ferromagnetic state as a consequence of a re-arrangement of magnetic moments.

Keywords: europium, ytterbium, magnetism, spin reorientation

(Some figures may appear in colour only in the online journal)

1. Introduction

Europium, cerium and ytterbium compounds show a great variety of anomalous physical phenomena, due to the different configuration of their *f*-electrons [1–4]. In particular, the phenomenon of valence instability is one of the most intensively studied through the possibility of Eu and Yb to fluctuate between divalent and trivalent ground states. The corresponding electron structures of these two states are Yb^{3+} ($4f^{13}$) / Yb^{2+} ($4f^{14}$) and Eu^{3+} ($4f^{6}$) / Eu^{2+} ($4f^{7}$).

In a systematic search for new compounds with Yb, interesting compounds have been synthesized and studied [5, 6]. Some of these are Yb_2Pd_2Sn and $YbPd_2In$. The former shows two quantum critical points under pressure [7] and under Sn/In doping [8], and the latter promises the record high heavy fermion [9].

Recently, we have started a systematic search of new ternary compounds in the analogous Eu-Pd-Sn system, motivated also by the fact that only two ternary compounds, EuPdSn and $EuPd_2Sn_2$, were known [10, 11]. In the course of our investigation several new compounds have been discovered, namely $Eu_3Pd_2Sn_2$, $EuPd_2Sn_4$ and $EuPdSn_2$, all showing a divalent magnetic state of Eu with complex magnetic structure [12, 13]. For example EuPdSn, which crystallizes in the TiNiSi-type, was reported by two different groups of researchers to order antiferromagnetically at 15.5 K with a further small anomaly in the magnetic susceptibility at lower temperatures [10, 14]. In fact, a neutron scattering study revealed a thermal evolution of the magnetic structure from a sine-wave modulated below T_N to planar helimagnetic at lower temperature [15]. Moreover, in both cases the antiferromagnetic structures are incommensurate. Other examples of complex magnetic behavior were found in Eu compounds belonging to similar Eu-*T*-*X* systems (T = transition metals, X = p-block elements) [16].

In this paper we report results on the crystal structure and the physical properties of the two isotypic compounds—$EuPdSn_2$ and $YbPdSn_2$.

Interestingly, both rare earths in these two compounds behave in the same chemical way, they are divalent with the equivalent large atomic volume. However, their magnetic behaviors are just opposed, being Eu^{2+} magnetic while Yb^{2+} non-magnetic. This feature makes $YbPdSn_2$ an appropriate reference compound to subtract the non-magnetic contributions from $EuPdSn_2$. A similar investigation was performed in cases of the analogous indides $EuPdIn_2$ and $YbPdIn_2$, which are isostructural with the stannides studied in our work, showing a divalent character for both Eu and Yb [17].

In the investigation of the isothermal section at 600 °C of the Yb-Pd-Sn system we reported the crystal structure of $YbPdSn_2$ [5, 6]. This compound was studied for the first time by Kussman and Pöttgen [18], although to date no data on physical properties are available. From a preliminary work [13], $EuPdSn_2$ was found to be isotypic with $YbPdSn_2$. Moreover, susceptibility measurements indicate a divalent magnetic state of Eu ions with a positive Weiss temperature and a cusp at 12.5 K indicating magnetic order.

2. Experimental details

$YbPdSn_2$ and $EuPdSn_2$ polycrystalline samples, each with a total weight of 1.2 g, have been prepared by weighing the stoichiometric amount of elements with the following nominal purity: Yb—99.993 mass % (pieces, smart elements GmbH, Vienna, Austria), Eu—99.99 mass % (pieces, smart elements GmbH, Vienna, Austria), Pd—99.5 mass % (foil, Chimet, Arezzo, Italy), Sn—99.999 mass % (bar, smart elements GmbH, Vienna, Austria). Due to very high oxidizability of elemental Eu, the $EuPdSn_2$ sample has been weighed inside a glove box. In order to avoid the loss of europium and ytterbium during the melting because of their high vapour pressure, the proper amounts of pure elements were enclosed in small tantalum crucibles sealed by arc welding under pure argon atmosphere. Pieces of the annealed samples were synthesized in an induction furnace under a stream of pure argon and annealed in a resistance furnace at 650 °C for three weeks for $YbPdSn_2$ and at 600 °C for two weeks for $EuPdSn_2$.

Finally the samples were quenched in cold water and characterized by optical and scanning electron microscopy (SEM) (EVO 40, Carl Zeiss, Cambridge, England), equipped with an electron probe microanalysis system based on energy dispersive x-ray spectroscopy (EPMA—EDXS). For the quantitative and qualitative analysis an acceleration voltage of 20 keV for 100 s was applied, and a cobalt standard was used for calibration. The x-ray intensities were corrected for ZAF (atomic number, absorption and fluorescence) effects. The annealed samples were crushed, powdered under pure acetone inside an agate mortar and studied by powder x-ray diffraction (XRD). The XRD data were collected at room temperature using the X-Pert MPD diffractometer (Philips, Almelo, The Netherlands) equipped with a graphite monochromator

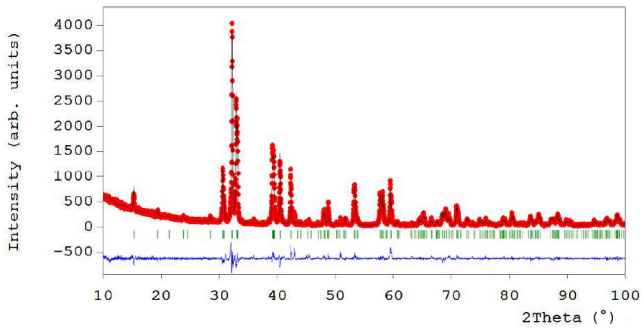

Figure 1. X-ray diffraction (CuK_α) powder pattern of $EuPdSn_2$. The experimental data are shown with circle symbols, while the solid line through the experimental points represents the Rietveld refinement. The indexed peaks associated to the crystal structure of $EuPdSn_2$ are displayed with the ticks and the lower curve represents the difference curve.

installed in the diffracted beam (Bragg Brentano, $CuK\alpha$ radiation). The theoretical powder pattern was calculated with the help of the Powder-Cell program [19]. The FULLPROF program [20] was used for Rietveld refinements. A Pseudo-Voigt profile shape function was used and full occupation with no atomic disorder was considered for all positions.

The thermodynamic and transport physical properties measurements were performed by a Physical Property Measurement System (PPMS) commercial device (Quantum Design) and PPMS Dynacool (Quantum Design) in the 2–300 K temperature range with applied magnetic field up to 9 T. Specific heat was determined by means of the relaxation 2-τ method. Electrical resistivity and magnetoresistance were measured using the 4-wire AC technique on irregular shapped samples in relative units. Magnetic properties were performed by a Magnetic Property Measurement System (Quantum Design) in the temperature range of 2–300 K under applied magnetic fields up to 9 T.

3. Experimental results

3.1. Crystal structure analysis and refinement of $EuPdSn_2$

From SEM/EPMA analyses the sample prepared for $EuPdSn_2$ resulted to be almost single phase with only some traces of an unknown phase of atomic composition 20% Eu, 30% Pd and 50% Sn which can therefore tentatively be described by the formula $Eu_2Pd_3Sn_5$. The XRD pattern of the $EuPdSn_2$ phase was successfully indexed by analogy with the corresponding already known orthorhombic phase $YbPdSn_2$, which crystallizes in $oS16$ structure $MgCuAl_2$-type (space group *Cmcm*), a ternary ordered version of the Re_2B type. The atomic positions of $YbPdSn_2$ were taken as starting values and the structure was successfully refined by using FULLPROF [20]. Final reliability factors of $Rp = 19.7\%$ and $\chi^2 = 2.51$ were obtained in the Rietveld refinement (see figure 1). The refined lattice parameters are $a = 0.4453(6)$, $b = 1.1590(8)$, $c = 0.7458(2)$ nm, whereas the atomic coordinates of $EuPdSn_2$ are shown in table 1. The few peaks unindexed of figure 1 very likely belong to $Eu_2Pd_3Sn_5$.

Table 1. Atomic coordinates of the novel compound $EuPdSn_2$ (space group *Cmcm*). Wyck. = Wyckoff position, Occ. = occupation number.

Atom	Wyck.	***x*/*a***	***y*/*b***	***z*/*c***	Occ.
Eu1	4*c*	0	0.4346(2)	1/4	1
Pd1	4*c*	0	0.7063(2)	1/4	1
Sn1	8*f*	0	0.1466(8)	0.0475(7)	1

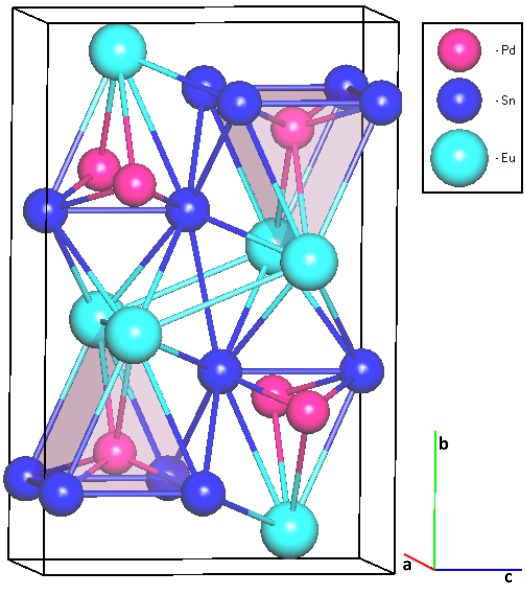

Figure 2. Representation of the $EuPdSn_2$ crystal structure onto the *bc* plane. The figure shows the topological layout of the Pd-centered trigonal prisms made of Eu and Sn atoms.

The $EuPdSn_2$ stannide structure can be described as a staggered net of trigonal prisms of composition $[Eu_2Sn_4]$ centered by a Pd atom (see figure 2).

3.2. Magnetic properties

In figures 3(a) and (b) the temperature dependencies of the magnetic susceptibilities $\chi(T)$ of $YbPdSn_2$ and $EuPdSn_2$, including respective $1/\chi(T)$ insets are shown. The measurements were done in a magnetic field of 0.1 T within the temperature range of 2–300 K. The two compounds exhibit Curie–Weiss (C-W) behaviour above 45 K for $YbPdSn_2$ and 15 K for $EuPdSn_2$. The susceptibility data for both compounds can be accounted for with a modified C-W law given by the equation

$$\chi(T) = \chi_0 + \frac{C}{T - \Theta_P}. \qquad (1)$$

From the high temperature fitting of the dependence $1/\chi(T)$ in the paramagnetic regime well above the T_N (shown in the insets of the figure) the values of effective magnetic moments μ_{eff} (computed from the Curie constant C), paramagnetic temperatures Θ_p and χ_0 Pauli susceptibilities for both the compounds were extracted.

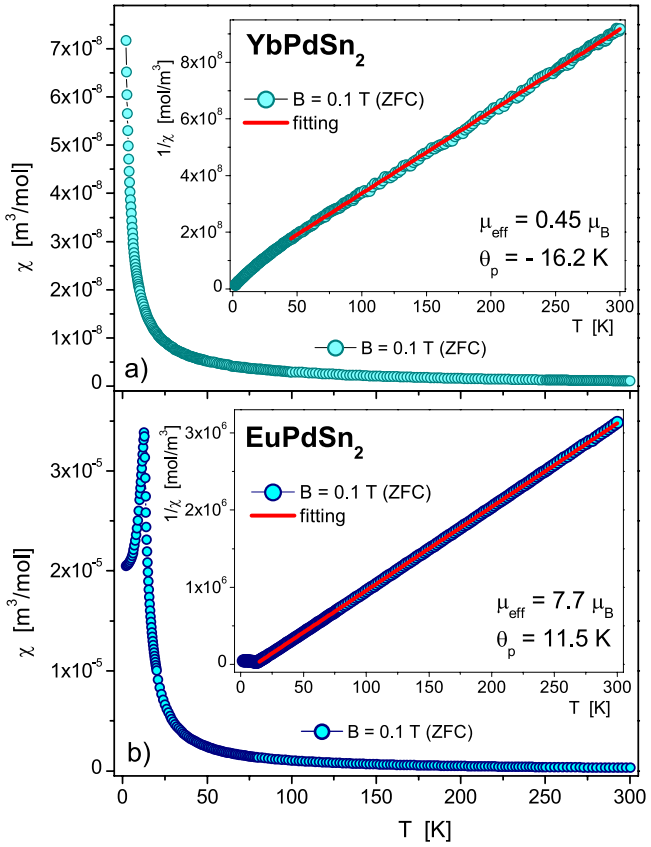

Figure 3. The temperature dependencies of magnetic susceptibility $\chi(T)$ for the $YbPdSn_2$ (a) and $EuPdSn_2$ (b), respectively. In the insets of both graphics the inverse susceptibilities $1/\chi(T)$ are plotted (the red lines represent the Curie–Weiss fitting function).

3.2.1. $YbPdSn_2$. The magnetic susceptibility of $YbPdSn_2$ is presented in figure 3(a). This compound shows typical C-W behaviour without any sign of magnetic ordering in the whole temperature range 2–300 K. From the fitting of $1/\chi(T)$ data we obtained a paramagnetic Weiss temperature Θ_p of -16.2 K and an effective magnetic moment of $\mu_{eff} = 0.45\ \mu_B$. The μ_{eff} is close to the theoretical zero value of Yb^{2+} (being equal that of Lu^{3+}). For a qualitative evaluation of the actual Yb valence in $YbPdSn_2$ compound one may use the ratio $\mu_{eff}(exp.)/\mu_{eff}(Yb^{3+}) = 0.45/4.54$. The resulting valence can be quantified as $2 + 0.45/4.54 = 2.1$. From the figure inset, one can notice that below $T \approx 50$ K the $1/\chi(T)$ dependence slightly turns downward due to crystal electric field (CEF) effect.

3.2.2. $EuPdSn_2$. The temperature dependence of the magnetic susceptibility $\chi(T)$ of $EuPdSn_2$ in the ZFC regime between 2–300 K is depicted in figure 3(b). In the inset of the figure the trend of inverse susceptibility is shown. The straight line of $1/\chi(T)$ of $EuPdSn_2$ down to low temperature (to about 15 K) shows no CEF effect according to a Eu divalent atom spin value of $S(= J) = 7/2$ and $L = 0$. The ZFC mode of collecting susceptibility data against temperature was compared with the FC mode and a negligible difference was found.

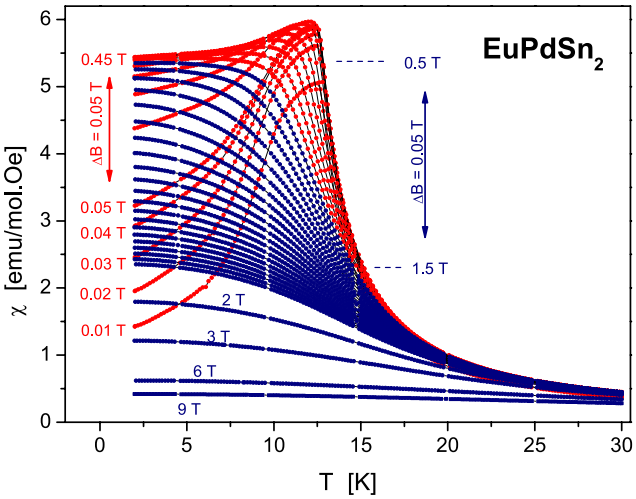

Figure 4. The low temperature (2–30 K) $\chi(T)$ magnetic susceptibility dependencies for different magnetic fields in the range 0.01–9 T (red curves for $B \leqslant 0.45$ T and blue ones for $B \geqslant 0.5$ T).

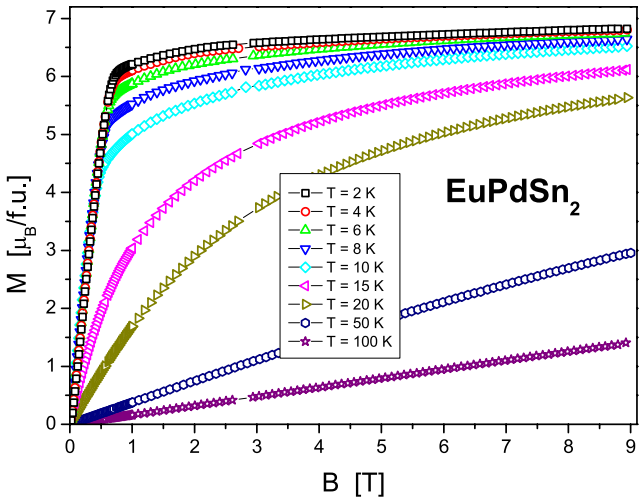

Figure 5. Magnetization as a function of magnetic field, M(B), of $EuPdSn_2$ at different constant temperatures in the temperature range of 2–100 K.

From the fitting of the $1/\chi(T)$ data we obtained a value of $\mu_{\text{eff}} = 7.7\ \mu_B$ which is close to the theoretical Eu^{2+} free-ion value of 7.94 μ_B, suggesting that Eu ions are in a divalent stable-moment magnetic state. The very low value of $\chi_0 = 4.10^{-10}$ m^3 mol^{-1} reveals a very small Pauli susceptibility, whereas the small but positive value of paramagnetic Weiss temperature $\Theta_p = 11.5$ K points to significant ferromagnetic correlations. At low temperatures, a distinct cusp at 12.5 K is observed in $\chi(T)$ of figure 3(b), indicating that $EuPdSn_2$ is magnetically ordered. Apparently, such a sharp cusp is symptomatic of antiferromagnetic ordering, however a more complex magnetic structure can not be excluded, mainly taking into account the observed positive Θ_p value. With the aim to describe the magnetic interactions in more detail, a series of $\chi(T)$ measurements were performed in the temperature range of 2–30 K for applied magnetic fields of 0–1.5 T with a $\Delta B = 0.05$ T, and in addition for $B = 2$ T, 3 T, 6 T and 9 T.

Figure 4 shows the low temperature $\chi(T)$ plots for $EuPdSn_2$. As one can see in the figure, for applied fields up to 0.45 T the susceptibility behavior is typical of antiferromagnetic order. It is interesting, however, that the phase transition temperature does not seem to shift at all between 0.01 T and 0.45 T. From about 0.5 T the thermal dependence of the susceptibility displays the characteristics of ferromagnetic behavior. This scenario of a field induced ferromagnetism is corroborated by the isothermal magnetization $M(B)$ at temperatures from 2 to 100 K shown in figure 5. In fact, whereas magnetization measurements above the ordering temperature of 12.5 K exhibit the typical field dependence described by a Brillouin function expected for a paramagnetic material, below the ordering temperature a kink in the $M(B)$ slope appears at the characteristic field $B = 0.45$ T. At 2 K the magnetization shows a saturation at approximately 6.8 μ_B/Eu atom which is close to the saturation moment of the free Eu^{2+} value of $gJ = 7\ \mu_B$/Eu.

Clarification of the magnetic ground state in $EuPdSn_2$ awaits neutron diffraction studies. We note, that complex magnetism is also found in monatomic EuPdSn [15].

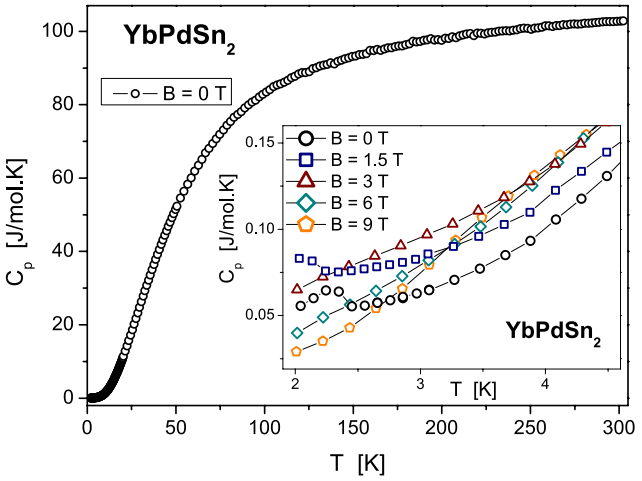

Figure 6. The temperature dependence of specific heat $C_p(T)$ of $YbPdSn_2$ compound. In the inset the low temperature part of $C_p(T)$ in different magnetic fields (0–9 T) is shown.

3.3. *Specific heat*

3.3.1. $YbPdSn_2$. The specific heat $C_p(T)$ of $YbPdSn_2$ was measured in the temperature range of 2–300 K and for magnetic fields 0–9 T. In figure 6 the $C_p(T)$ dependence in zero magnetic field in the whole temperature range is shown. At room temperature, $C_p(T)$ tends to the $3nR$ value expected from the Dulong–Petit law, being n the number of atoms in the formula unit and R the gas constant. In the inset, the low temperature detail for selected magnetic fields is presented. $C_p(T)$ dependence in $B = 0$ T for $YbPdSn_2$ shows a simple behaviour without any sign of bulk magnetic ordering down to 2 K. The small anomaly at $T = 2.3$ K, which is suppressed by increasing of magnetic field, is probably due to the presence of a trace amount of a trivalent ytterbium oxide Yb_2O_3 [21, 22]. The electronic Sommerfeld coefficient at $B = 0$ is $\gamma \approx 20$ mJ mol$^{-1} \cdot$ K^2. The specific heat of $YbPdSn_2$ is very slightly influenced by applied magnetic field up to 9 T (see the inset of figure 6), which implies a negligible magnetic

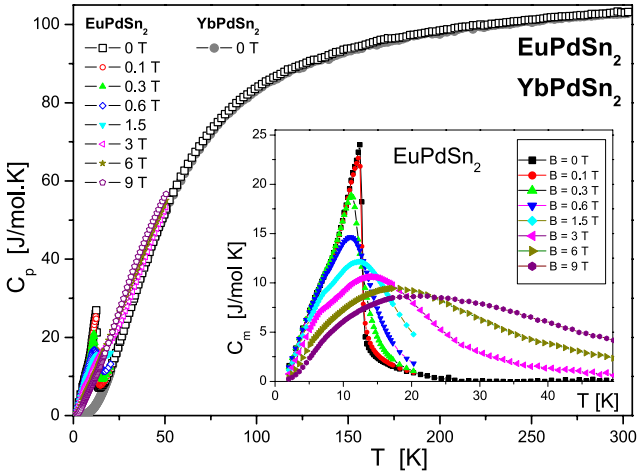

Figure 7. The specific heat $C_p(T)$ of $EuPdSn_2$ in different magnetic fields 0–9 T. For comparison the $C_p(T)$ of $YbPdSn_2$ at $B = 0$ T (gray colour circles) is also plotted. In the inset the $C_m(T)$ low temperature detail is shown.

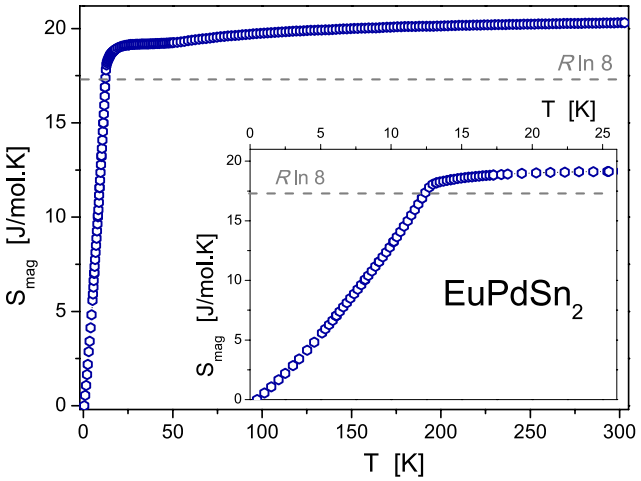

Figure 8. The temperature variation of the magnetic entropy $S_{mag}(T)$ of $EuPdSn_2$. Inset: the low temperature detail (0–25 K) of $S_{mag}(T)$ dependence.

contribution to specific heat. Such a behaviour is well known for ordinary metals in the absence of a magnetic phase transition.

3.3.2. $EuPdSn_2$. In figure 7 the high temperature dependence of specific heat $C_p(T)$ for $EuPdSn_2$ is presented and compared with that of $YbPdSn_2$.

Although it is not possible to extract the electronic band contribution in $EuPdSn_2$ in a direct manner, taking into account that $YbPdSn_2$ behaves as its equivalent non-magnetic reference, the free electron contribution for $EuPdSn_2$ can be supposed with the same value $\gamma \approx 20$ mJ mol^{-1} K^2.

In the inset of figure 7 the low temperature part of the magnetic specific heat $C_m(T)$, for different magnetic fields up to 9 T, is shown (phonon contribution was substracted taking the specific heat of non-magnetic $YbPdSn_2$). At zero magnetic field the plot shows a λ-like anomaly at 13 K. For magnetic fields below a certain threshold (B_{thr} within 0.6 T and 1.5 T) the curves intersect in a fixed point indicating that the $C_m(T)$ variation is dominated by the same mechanism of magnetic interactions. Above B_{thr} the effect of magnetic field takes over and the maximum of $C_m(T)$ shifts to higher temperatures and becomes broader. This latter behavior is usually found for ferromagnetic order, in agreement with isothermal magnetization $M(B)$ and susceptibility $\chi(T)$ measurements. A possible scenario would be that of a non collinear antiparallel arrangement of magnetic moments at $B = 0$, that continuously turn to collinear up to $B = B_{thr}$.

A shoulder at $\approx$7 K is also present in $C_m(T)$. As one can see from the inset of figure 7, the intensity of this anomaly remains practically unchanged up to ≈ 1.5 T and then weakens with increasing magnetic field, while its location remains unchanged at constant temperature. This shoulder could be attributed to the presence of the spurious phase $Eu_2Pd_3Sn_5$ found in the traces, although a significant amount of such phase is expected to produce this effect. Therefore this is more probably caused by change of magnetic structure of the title compound. This possibility should be proved using spectroscopic techniques.

The magnetic contribution to the entropy $S_{mag}(T)$ follows from $S_{mag} = \int_0^T \frac{C_{mag}(T')}{T'} dT'$. In order to subtract the phonon contribution and obtain the C_{mag} temperature dependence of $EuPdSn_2$, the non magnetic $YbPdSn_2$ counterpart was used. As shown in figure 8 the entropy saturates at around 20.3 J mol^{-1} K^{-1} which is close to $R\ln(2J+1) = R\ln 8 = 17.28$ J mol^{-1} K^{-1}. This value is in agreement with the expected Hund's rule octet ground state for $J = S = 7/2$, where $L = 0$ inhibits CEF effects independently of the point symmetry as is the case also for Gd^{3+} ions. The $\approx$15% of excess in the computed entropy value can be attributed to a slight difference between the phonon spectra of $EuPdSn_2$ and $YbPdSn_2$, because the phonon entropy already duplicates magnetic one $S_{mag} = R\ln 8$ at the Debye temperature.

3.4. Electrical resistivity

The measurements of electrical resistivity $\rho(T)$ were done on $YbPdSn_2$ and $EuPdSn_2$ samples of irregular shape, therefore the $\rho(T)$ values are plotted in arbitrary units. Both samples show high values of residual resistivity ratio (RRR) (for $YbPdSn_2$ RRR = 43, for $EuPdSn_2$ RRR = 30). These values confirm the good crystalline quality of the prepared samples.

3.4.1. $YbPdSn_2$. Figure 9(a) exhibits the low temperature region of electrical resistivity $\rho(T)$ of $YbPdSn_2$ for different magnetic fields and in the inset the whole temperature range 2–300 K is shown. No bulk pronounced anomalies were detected down to 2 K. In the main panel one can see the dropping of $\rho(T)$ at around 3.8 K caused by a tiny amount of elemental Sn being superconducting at $T_c = 3.72$ K, with a critical field of $B_c = 0.03$ T [23, 24]. The graph presents the $\rho(T)$ in $B = 0.05$ T where this effect is completely annihilated.

3.4.2. $EuPdSn_2$. In figure 9(b) the low temperature detail of temperature dependence $\rho(T)$ of $EuPdSn_2$ in different magnetic fields up to 9 T is shown. The resistivity decreases monotonously with decreasing temperature as is typical for ordinary metals. An abrupt decrease at about 12.5 K occurs owing to magnetic ordering. This feature is suppressed for magnetic fields above 3 T. This behaviour is in agreement with the $\chi(T)$ and $C_p(T)$ experimental results.

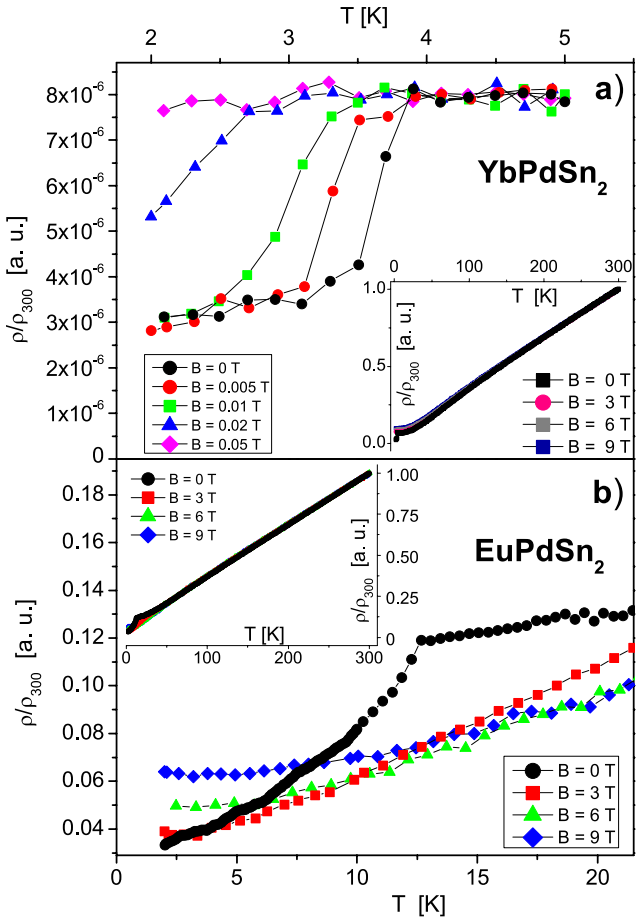

Figure 9. The low temperature detail of normalized electrical resistivity $\rho(T)$ in different magnetic fields for $YbPdSn_2$ and $EuPdSn_2$ in (a) and (b), respectively. In the insets of the graphs for both samples the $\rho(T)$ in whole measured temperature range 2–300 K is presented.

By increasing magnetic field one can see a small increase of the residual resistivity which can be attributed to the Zeeman splitting to the eight-fold ground state.

4. Conclusions

The two isotypic compounds $YbPdSn_2$ and $EuPdSn_2$ have been synthesised and magnetic, thermal and transport properties have been studied. In both stannides a divalent state of the rare earth was found. This makes $EuPdSn_2$ a magnetic compound and $YbPdSn_2$ a simple paramagnetic an appropriate reference compound that enables to access the 4*f* electron magnetic character of $EuPdSn_2$.

A careful series of magnetic susceptibility $\chi(T)$ measurements performed at different magnetic fields on $EuPdSn_2$ indicate that at weak magnetic fields ($B < 0.5$ T) this compound is antiferromagnetic (possibly with a non-collinear arrangement of magnetic moments) with a Néel temperature of $T_N = 12.5$ K. With increasing magnetic fields a continuous re-arrangement of magnetic moments towards a ferromagnetic-like state was found. Measurements of isothermal magnetization $M(B)$ and specific heat $C_p(T)$ support this scenario. In particular, $C_p(T)$ plots at different magnetic fields intersect in the fixed point for weak fields, whereas for $B > 0.6$ T $EuPdSn_2$ behaves ferromagnetically.

Acknowledgments

This work was partially supported by the projects VEGA 1/0956/17, VEGA 1/0611/18 and APVV-16-0079. AMS thanks the SA—NRF (93549) and the URC/FRC of UJ.

ORCID iDs

I Čurlík https://orcid.org/0000-0003-4889-0535
M Giovannini https://orcid.org/0000-0003-7983-2437
A M Strydom https://orcid.org/0000-0003-2117-5921

References

[1] Steglich F and Wirth S 2016 *Rep. Prog. Phys.* **79** 084502
[2] Carretta P, Giovannini M, Horvatic M, Papinutto N and Rigamonti A 2003 *Phys. Rev.* B **68** 220404(R)
[3] Wu L S *et al* 2016 *Science* **352** 1206–10
[4] Carretta P, Pasero R, Giovannini M and Baines C 2009 *Phys. Rev.* B **79** 020401(R)
[5] Giovannini M, Pasero R and Saccone A 2010 *Intermetallics* **18** 429–33
[6] Gastaldo F, Giovannini M, Strydom A, Djoumessi R, Čurlík I, Reiffers M, Solokha P and Saccone A 2017 *J. Alloys Compd.* **694** 185–92
[7] Muramatsu T *et al* 2011 *Phys. Rev.* B **83** 180404(R)
[8] Bauer E *et al* 2005 *J. Phys. Condens. Matter* **17** S999–1009
[9] Gastaldo F, Džubinská A, Reiffers M, Pristáš G, Čurlík I, Sereni J G and Giovannini M 2017 (arXiv:1711.02335v1 [cond-mat.str-el])
[10] Adroja D T and Malik S K 1992 *Phys. Rev.* B **45** 779–85
[11] Schwickert C, Winter F and Pöttgen R 2014 *Z. Nat.forsch.* B **69** 775–85
[12] Solokha P, Čurlík I, Giovannini M, Lee-Hone N, Reiffers M, Ryan D and Saccone A 2011 *J. Solid State Chem.* **184** 2498–505
[13] Čurlík I, Gastaldo F, Giovannini M, Strydom A and Reiffers M 2017 *Acta Phys. Pol.* A **131** 1003–5
[14] Müllmann R, Ernet U, Mosel B, Eckert H, Kremer R, Hoffmann R D and Pöttgen R 2001 *J. Mater. Chem.* **11** 1133–40
[15] Lemoine P, Cadogan J, Ryan D and Giovannini M 2012 *J. Phys.: Condens. Matter* **24** 236004
[16] Latka K, Przewoźnik J, Verbovytskyy Y and Gonçalves A 2015 *J. Alloys Compd.* **650** 572–7
[17] Galadzhun Y, Hoffmann R D, Kotzyba G, Künnen B and Pöttgen R 1999 *Eur. J. Inorg. Chem.* 975–9
[18] Kußmann D and Pöttgen R 2001 *Z. Nat.forsch.* B **56** 446–8
[19] Kraus W and Nolze G 1996 *J. Appl. Crystallogr.* **29** 301–3
[20] Rodríguez-Carvajal J 1993 *Phys. B: Condens. Matter* **192** 55–69
[21] Adachi G, Imanaka N and Kang Z 2004 *Binary Rare Earth Oxides* (Berlin: Springer) p 257
[22] Bonrath H, Hellwege K H, Nicolay K and Weber G 1966 *Phys. Kondens. Mater.* **4** 382–90
[23] Matthias B T, Geballe T H and Compton V B 1963 *Rev. Mod. Phys.* **35** 414
[24] Eisenstein J 1954 *Rev. Mod. Phys.* **26** 277–91